FARADAY

Rotating waves on disk and ring electrodes

Ralph D. Otterstedt,[a] Peter J. Plath,[a] Nils I. Jaeger[a]* and John L. Hudson[b]

[a] *Institut für Angewandte und Physikalische Chemie, Universität Bremen, FB 2 D-28334 Bremen, FRG*

[b] *School of Engineering and Applied Science, Department of Chemical Engineering, University of Virginia, Charlottesville, VA, 22903, USA*

Experimental studies have been carried out with cobalt disk and ring electrodes in buffered phosphate solutions under potentiostatic control with the Haber–Luggin capillary of the reference electrode placed in the centre of the electrode close to the surface.

The applied potential is adjusted to be cathodic with respect to the Flade potential. Visible fronts outlining a propagating wave and characterizing the transition from the passive to the active state of the metal rotate around the tip of the reference electrode while the overall measured current remains almost constant. At applied potentials close to the Flade potential a modulation of the rotating wave and, correspondingly, of the current time curves, is observed.

Oscillating electrochemical reactions have been known for a long time: in particular, current oscillations under potentiostatic control during the electrodissolution of metals in the transition region between the active and the passive state have been studied in great detail.[1,2] Oscillations in the cobalt–phosphoric acid system have been reported previously[3] and studied in detail in ref. 4–6.

The observation of spatiotemporal phenomena on electrode surfaces accompanying oscillations have been investigated only recently, while spatiotemporal patterns in homogeneous reaction–diffusion systems[7] and on various levels of heterogeneous catalytic systems[8] are well established experimentally and in mathematical models.

Lev *et al.*[9] have shown that current oscillations on a potentiostatically controlled nickel wire in sulfuric acid in the transpassive region are accompanied by travelling current–density waves. The phenomenon has been modelled by the same group.[10,11] Spatiotemporal period doublings and other spatiotemporal phenomena were observed during the electrodissolution of iron in sulfuric acid by Hudson *et al.*[12] and by Sayer and Hudson.[13]

Spatiotemporal structures have been observed during cobalt electrodissolution by Otterstedt *et al.*[14] The propagation, acceleration and backfiring of pulses has been observed on cobalt wires in the bistable, oscillating and excitable regime of the system.[15,16]

Flätgen and Krischer[17] have observed accelerating fronts on a silver ring electrode in an electrocatalytic reaction. The authors have shown that non-local coupling effected by migration currents parallel to the electrode surface gives rise to the observed acceleration.[17,18]

In the case of the cobalt–buffered phosphoric acid system, the observed acceleration of propagating activation fronts can also be ascribed to a non-linear dependence of the rate of oxide dissolution upon the distance of the electrode potential relative to the Flade potential.[15]

In this paper, we report on active areas rotating with constant angular velocity on cobalt disk and ring electrodes under the constraint of a symmetric arrangement of reference and counter electrodes which gives rise to a radial dependence of the potential drop across the double layer and oxide film on the disk.

With the applied voltage close to the Flade potential, the phenomenon of modulation can also be observed in this system.

Experimental

The experimental set-up is shown in Fig. 1. Experiments were carried out in a buffered phosphoric acid electrolyte (1 mol dm^{-3}, pH 1.67) prepared by dissolving 85% phosphoric acid and dipotassium hydrogenphosphate in deionized water.

A common three-electrode configuration was used. Potentiostatic experiments were controlled by an EG&G potentiostat. The working electrode was made from a 12.5 mm diameter cobalt rod (Johnson Matthey) embedded in a Teflon cylinder. The ring electrode was prepared by sealing the centre part of the disk with adhesive tape leaving an outer ring with a width of 1.25 mm. For a symmetric electrode arrangement

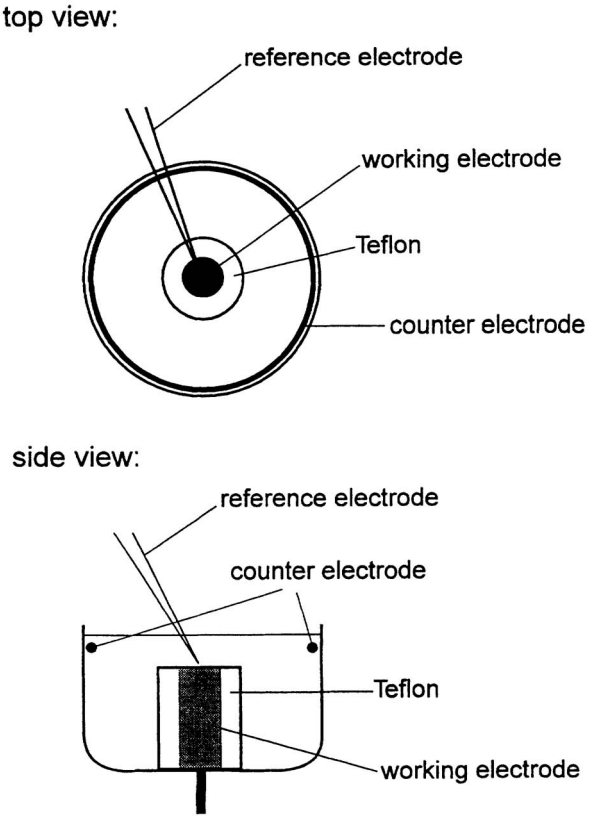

Fig. 1 Experimental set-up

the counter electrode made from 2 mm diameter copper wire was bent to a circle of 70 mm in diameter and located in the same plane around the working electrode. The Haber–Luggin capillary of the calomel reference electrode with a tip diameter of about 100 μm was placed 1 mm away from the surface in the centre of the disk. The solution level was located 10 mm above the electrode surface. Prior to each experiment, the electrode was sanded wet with grit 400 and grit 2400 sand paper and then cleaned in distilled water in an ultrasonic bath. Video images were taken with a commercial camcorder and subsequently digitized.

Results

Disk experiments

The rotating wave investigated in this work consists of an area of active metal electrodissolution (high current density) which propagates on a passive surface (low current density). The transition occurs as the electrode potential is moved into the cathodic direction with respect to the Flade potential which itself depends on the pH of the electrolyte.[19]

Depending on the cathodic distance of the electrode potential with respect to the Flade potential and on the conductivity of the electrolyte, the cobalt–buffered phosphoric acid system can be in a bistable state, an oscillatory state or in an oscillatory state showing the phenomenon of modulated travelling waves.[15,16] As a prerequisite prior to the investigation of the dynamic behaviour of the electrode, the position of the Flade potential has to be determined. A value of 1038 mV *vs.* SCE has been determined for the 1 mol dm^{-3} buffered phosphoric acid electrolyte of pH 1.67. Details of the experimental procedure have been reported elsewhere.[15]

The experiment is started by stepping the rest potential of the metal electrode to a value between 500 and 1000 mV *vs.* SCE, *i.e.* keeping it below the Flade potential. While the centre of the electrode around the tip of the reference electrode remains active, the rest of the surface of the disk attains a passive state.

After the potential is stepped from the rest potential to the value of the experiment, a current overshoot is followed by passivation of most of the electrode surface and a drop of the current to a low value. Thereafter a small circular active area begins to develop, starting at the centre of the disk. The diameter of the area grows and moves toward the rim of the electrode. At the same time the current starts to rise again. The propagating visible front marks the border between the passive and the active area on the electrode. At some point of this activation process the ring becomes asymmetric and the asymmetry grows until the closed front touches the rim of the electrode, where it breaks up into two branches. The beginning of the experimental observation is summarized in a schematic drawing (Fig. 2). The figure is a close-up of the cobalt disk electrode with the expanding active area depicted in black. Only one of the two branches continues to move clockwise or counterclockwise around the tip of the reference electrode whereas the other one remains stationary. This branch no longer marks an active/passive border. It disappears from the surface when the second, circling branch passes by completing the first rotation. The period of the observed rotations is of the order of 30–50 s in the stationary state which is established after about twelve rotations. At this point the current has reached an almost constant value. The period increases during the first rotations and for potentials closer to the Flade potential, *e.g.* 40 s for V_{appl} = 750 mV, 50 s for 850 mV in the stationary state. The rotating wave appears also when the potential is slowly scanned rather than stepped from the rest potential.

Fig. 3(a) shows the digitized images of the front of a clockwise rotating wave for an applied potential of 800 mV *vs.* SCE. The curvature of the front is stable in time. Fig. 3(b) depicts the current–time series of this experiment for four rotations of the front after a stationary period has been established. The small modulation of the current will be discussed in the context of the ring experiments. There is an almost constant active area moving around the tip of the capillary. This assumption is supported by a potential measurement with a reference electrode placed at a point near the rim of the electrode shown in Fig. 3(c). The signal of the auxiliary reference electrode indicates a transition from the passive to the active state and back during the passage of the front. The potential at the rim is more anodic than the applied potential (1200 mV *vs.* SCE as opposed to 850 mV *vs.* SCE), shifts to more cathodic values when the (black) front passes by and returns afterwards to its initial value. The passage of the wave is marked by sharp changes in the current density and hence of the ohmic potential drop in the electrolyte. With the rotating visible front (period of rotation is 35 s) approaching the position of the auxiliary reference electrode the potential starts to move into the cathodic direction. The most cathodic value (100 mV *vs.* SCE) is established behind the propagating front for *ca.* 5 s. Thereafter the potential starts to rise again indicating repassivation. The transition on either side of the wave is smooth. The time needed for the passage of the wave is estimated from the half width of the signal in Fig. 3(c) to be *ca.* $\frac{1}{4}$ of the period of rotation. This corresponds to a segment of active electrodissolution covering *ca.* $\frac{1}{4}$ of the area on the disk.

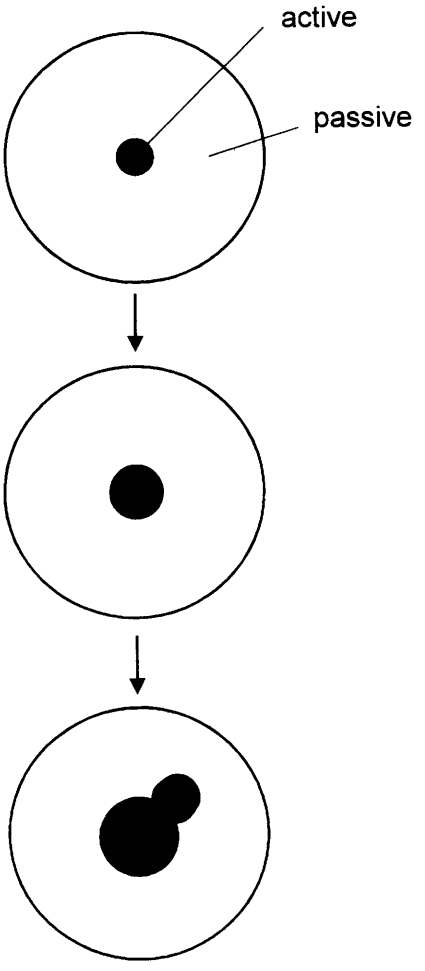

Fig. 2 Schematic representation of the activation process on the electrode

At an applied potential of 950 mV *vs.* SCE, a modulation of the wave can be observed.[16] Fig. 4 depicts the leading edge of the wave rotating counterclockwise [L in Fig. 4(a)]. As the active area propagates, it expands intermittently into the

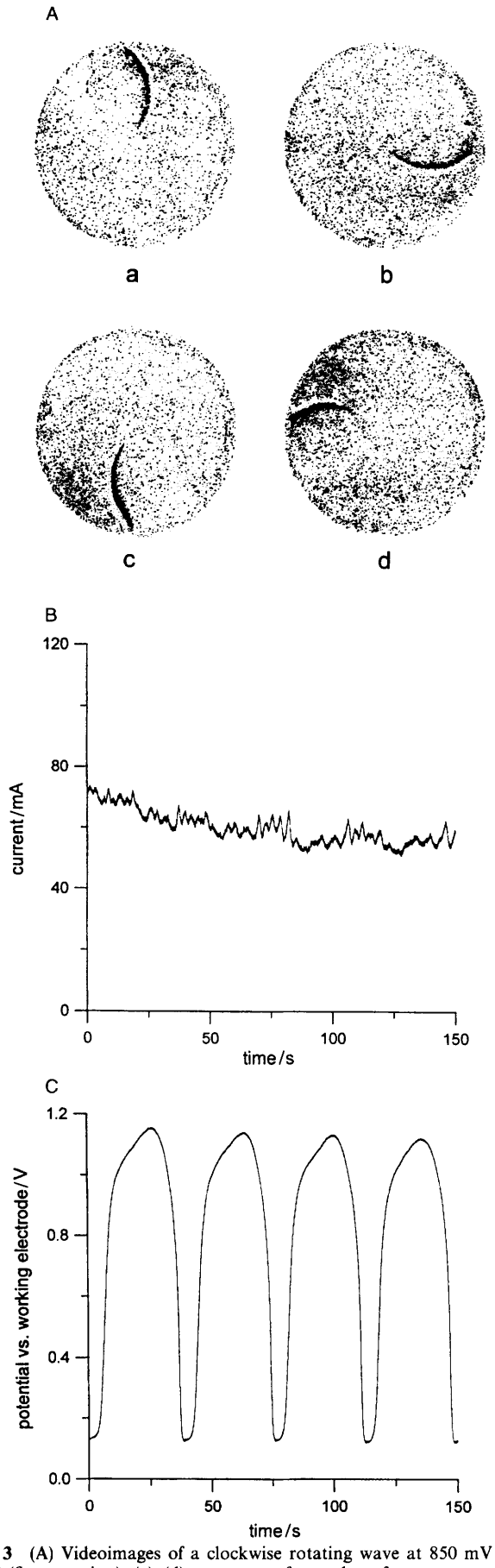

Fig. 3 (A) Videoimages of a clockwise rotating wave at 850 mV *vs.* SCE (first rotation); (a)–(d): sequence of snapshots for every quarter of the rotation. (B) Current–time curve of the rotating wave at 850 mV *vs.* SCE. (C) Potential between the working electrode and an additional calomel reference electrode with a capillary placed at the rim of the working electrode *ca.* 1 mm away from the surface.

reverse direction. Each time a modulation or breathing occurs, the activation front moving in the reverse direction is also visible. The black visible front is eventually arrested (**B**, b in Fig. 4) where the expansion of the active area ends and the contraction begins. These arrested fronts are visible in Fig. 4. They correspond to the visible stationary branch described for the asymmetric activation process. Again, the black lines are removed upon the passage of the main front. In Fig. 4(d) more than nine arrested fronts can be seen, *i.e.* the frequency of modulation is approximately nine times the frequency of rotation of the main pulse. Fig. 5 shows the modulation of the current corresponding to the modulation of the wave. These modulated waves appear to be similar to the modulated travelling waves seen previously by Bayliss *et al.* in cellular flames;[20] for a discussion of the properties of modulated travelling waves see, for example, Brown and Kevrekidis.[21]

At an applied potential of 1000 mV *vs.* SCE *i.e.* even closer to but still cathodic to the Flade potential, only a stationary circular front develops, separating the active centre part of the electrode around the tip of the reference electrode from the passive area around it. It corresponds to the initial situation depicted in the schematic drawing (Fig. 2).

Ring experiments

Fig. 6(a) shows the digitized images of the front of a wave rotating counterclockwise with a period of 9 s for an applied voltage of 700 mV *vs.* SCE. The velocity of the visible front is not as constant as in the case of the disk and the current–time series for the first three cycles [Fig. 6(b)] shows corresponding more or less periodic current modulations. After five cycles the observable front disappears while the current remains constant.

Occasionally, *e.g.* at an applied potential of 950 mV *vs.* SCE, which is close to, but not too close to the Flade potential (1038 mV *vs.* SCE), there may occur after some rotations of a single wave a second one rotating in the opposite direction. When the leading visible edges of the waves meet they both disappear and the current reaches a maximum. Thereafter the active area contracts and the current reaches a minimum. Then a new wave arises quickly and starts to propagate along the ring, *i.e.* the remaining active area starts to rotate again. Eventually, a second one appears again giving rise to the complex current–time curve depicted in Fig. 7. It is not clear at the present time whether or not the second wave splits off the first one.

For an applied potential of 1000 mV *vs.* SCE, *i.e.* closer to the Flade potential, the phenomenon of modulation of the wave occurs also in the ring geometry. The corresponding current–time series (Fig. 8) shows the current oscillating with the periodicity of the modulation. The velocity of the leading front of the active area is not stationary, hence the different amplitudes of the peaks in the current–time curve (Fig. 8). The period of rotation is 24 s for the first rotations.

Discussion

The appearance and the properties of the rotating wave depend on the applied potential (V_{appl}). It is the sum of the potential drop across the electric double layer including the passive film in the position of the reference electrode at the centre of the disk and the ohmic potential drop between the working electrode and the tip of the capillary of the reference electrode in the electrolyte.

In order to maintain the desired potential between the working and the reference electrode (V_{appl}) the potentiostat has to supply a higher voltage between the working and the counter electrode in order to compensate for the ohmic potential drop between the reference electrode and the counter electrode caused by the current flowing toward the counter

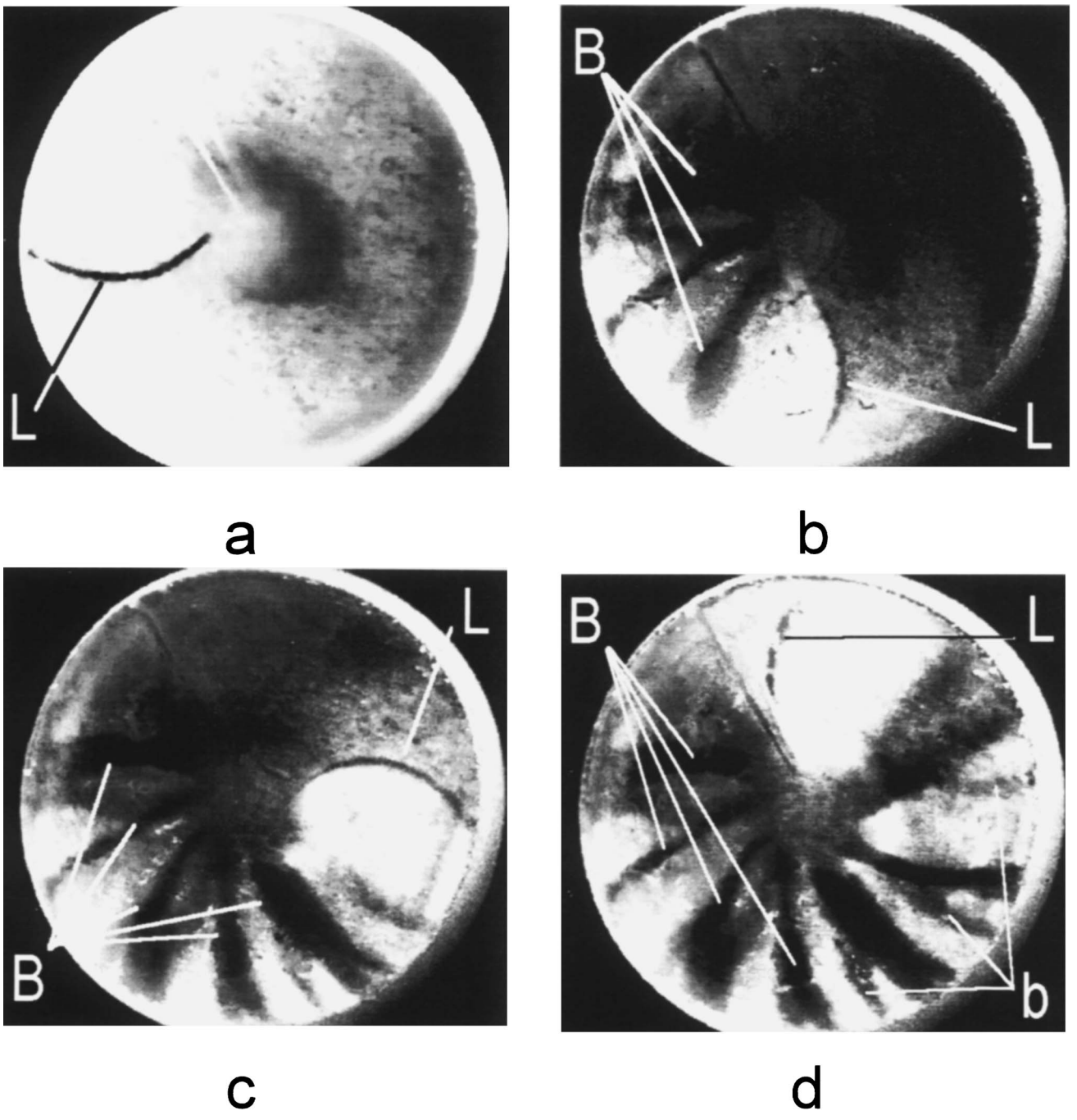

Fig. 4 Digitized video images of the modulated counterclockwise rotating wave. L denotes the position of the moving visible edge; B and b denote the positions where the backward propagation of the tail of the wave has stopped. (a)–(d): sequence snapshots for every quarter of the rotation.

electrode. The voltage V between working and counter electrode is the sum of V_{appl} at the position of the reference electrode and the ohmic potential drop V_Ω between counter and reference electrode: $V = V_{appl} + V_\Omega$. It is constant in the stationary state.

With the working electrode at ground zero, the potential drop across double layer and passive film will increase in the radial direction from the centre of the disk. This is due to the circular geometry of the electrode arrangement. It causes a redistribution of V in favour of an increasing proportion across the double layer in a radial direction outward. If at some distance from the centre the Flade potential is exceeded, the electrode will attain the passive state. A schematic representation assuming an arbitrary dependence of the potential drop across oxide film and double layer on the radial position is given in Fig. 9 for a symmetric situation.

In an ideal circular symmetric system a marginally stable steady state situation with a circular boundary between the active and the passive part of the electrode could be expected. The integral current should approach a constant value corresponding to a constant active area as long as the situation at the position of the reference electrode does not change. The size of the active area is determined by the applied voltage at the centre of the electrode.

The visible front separating the active and the passive part is marked by a sharp jump in the current density and hence in the ohmic potential drop in the electrolyte [Fig. 3(c)]. As can be also seen from the figure, the active area remains constant as the pulse rotates around the disk. This indicates that a pseudo steady state has been reached. A true steady state is never reached in these experiments since the surface of the electrode is slowly changing; nevertheless, the surface changes

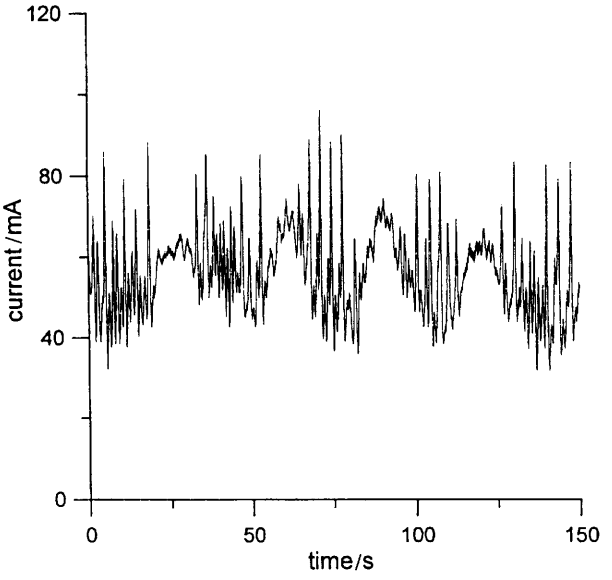

Fig. 5 Current–time curve of the modulated rotating wave at 1000 mV *vs.* SCE.

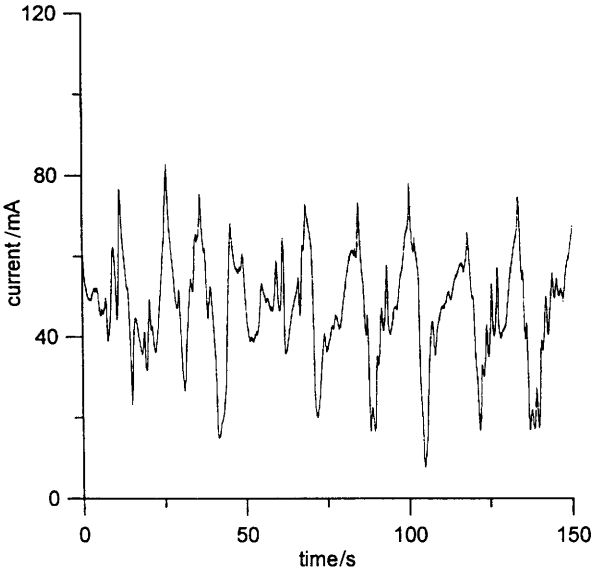

Fig. 7 Current–time curve of two counter rotating waves on the ring electrode

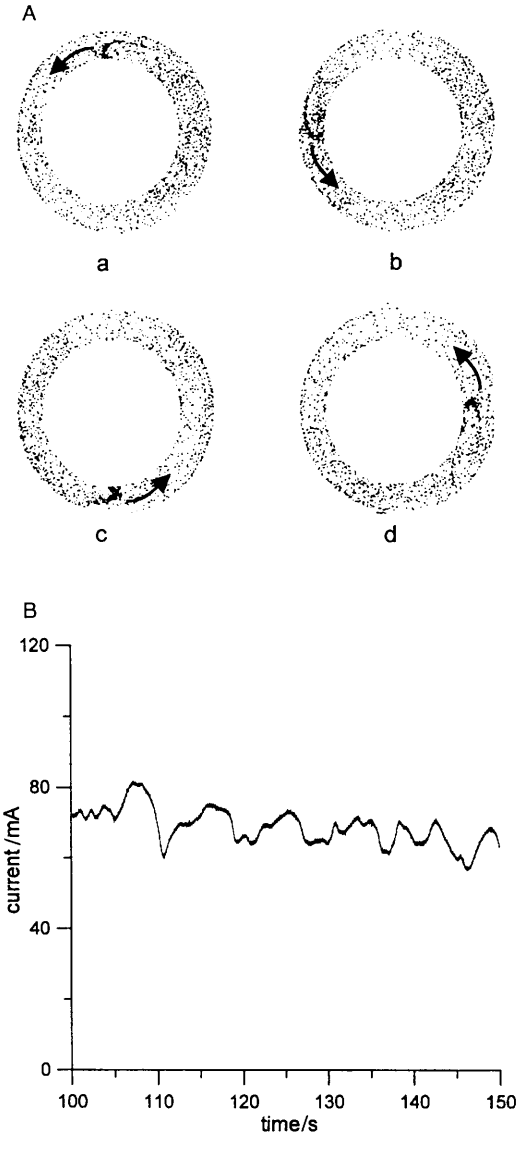

Fig. 6 (A) Digitized video images of a single counterclockwise rotation wave on the electrode at 700 mV *vs.* SCE; period of rotation: 9 s; (a)–(d): sequence of snapshots for every quarter of rotation; the arrow denotes position and direction of propagation of the wave. (b) Current–time curve of the single wave on the ring electrode.

are slow compared with the timescale of the dynamics.

The nature of the black front is not known at the present time. It can be assumed that it consists of an intermediate precipitate which is removed as the activation process is completed. This can be observed, when the circling pulse passes the black line which was left stationary at the beginning of the rotation of the pulse. The moving front can be arrested and remains visible upon opening the circuit thus moving the electrode back to the rest potential with no current flowing. A density gradient in the electrolyte across the active-passive interface, which can be expected due to different rates of electrodissolution, can therefore be ruled out as a reason for the visibility of the moving front.

Non-local coupling due to the potential gradient (electric field) established across the boundary between the active and the passive part of the electrode plays a major role in the propagation of the wave front in the tangential direction. The potential across the passive film near the boundary is shifted into the direction cathodic of the Flade potential and therefore the electrodissolution of the passive film will start. This has been discussed in detail in ref. 16. The steady state

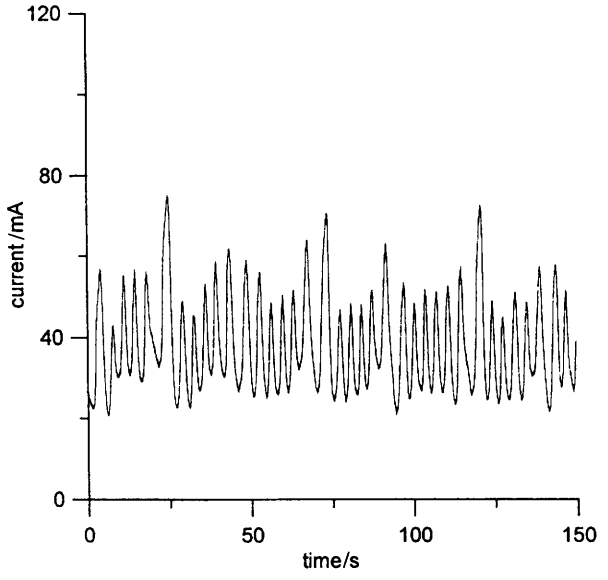

Fig. 8 Current–time curve of the modulated wave on the ring electrode

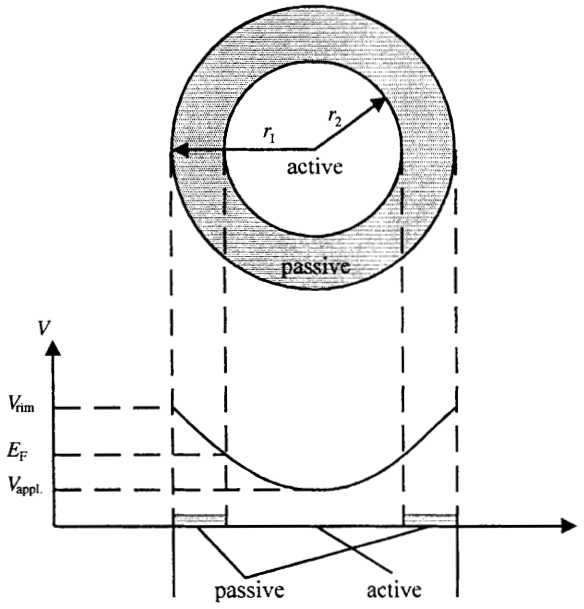

Fig. 9 Qualitative dependence of the potential drop on the radial position and hypothetical coverage with a passive layer. V_{rim}: potential at the rim of the working electrode; E_F: Flade potential; V_{appl}: applied potential.

requires that an advance of the wave has to be compensated by repassivation in the back of the wave.

An increase of the period on ring and disk has been observed for V_{appl} at the centre of the electrode increasing into the anodic direction toward the Flade potential. This can be understood by assuming a decreasing potential gradient in tangential direction across the active/passive boundary. Owing to the lower current flowing, the potential drop across the double layer on the active part of the surface is less and the voltage V between counter and working electrode is smaller as well, *i.e.* the potential gradient and hence the non-local coupling is decreased.

Repassivation occurs upon the passage of the pulse as can be seen by the increase of the potential back into the region of passivity [Fig. 3(c)].

The mechanism of repassivation is not known at the present time. It is assumed that porous layers of higher oxides are precipitated by hydrolysis and oxidation of cobalt ions which are formed with a high rate. Owing to the large current density, hydrogen ions will migrate out of the pores of the layer. The resulting increase in pH will shift the Flade potential into the cathodic direction. As soon as the Flade potential is cathodic with respect to the potential drop across the double layer, repassivation can occur. This mechanism has been discussed in detail for current oscillations on the limiting-current plateau in the electrodissolution of iron in sulfuric acid by Russell and Newman.[22] Possible mechanisms of oxide formation and dissolution have been discussed by Sazou and Pagitsas in order to explain the appearance of current oscillations in the cobalt–phosphoric acid system.[6]

With the applied potential at the centre of the disk moved closer to the Flade potential, a modulation of the propagating wave can be observed (Fig. 4 and 5). The rotating active sector periodically expands in the direction opposite to the rotation. In order to explain this phenomenon, reference is again made to the pH dependence of the Flade potential.

The Flade potential of a metal depends on the pH of the solution according to the relationship: $E_F = E_{0,\,metal} + RT/nF \ln a_{H+}^{\nu}$ where ν is the stoichiometric coefficient and n the number of electrons in the electrode reaction.[19,23] As the surface is activated, hydrogen ions migrate away from the active surface toward the counter electrode. This leads to a local increase of the pH and as a consequence to a shift of the Flade potential into the cathodic direction. The pH dependence of the Flade potential in the buffered cobalt–phosphoric acid electrolyte was determined to be 118 mV per pH unit.[15] In the case where the Flade potential is cathodic with respect to the potential drop across the double layer, the surface begins to repassivate after the activation front has passed. This follows a hypothesis forwarded by Franck and FitzHugh[24] to model the oscillations in the case of iron in sulfuric acid.

An expanding active area and hence an increasing total current will shift the applied potential in dependence on the radial position on the disk into the anodic dierection. If, owing to migrating hydrogen ions away from the electrode, the Flade potential will shift into the cathodic direction at the same time, the condition for repassivation is reestablished. The passive film formed behind the moving front will be very thin and shortly after it has been formed it will begin to be removed by the same mechanism which drives the primary leading edge. The active area contracts and expands and the current decreases and increases on a faster timescale compared with the rotation of the wave. The feedback in the system is due to the ohmic potential drop in the electrolyte. The expansion of the active area into the direction opposite to the leading front is observable by a moving visible front and occurs on a faster timescale. This can be inferred from Fig. 5. The current spikes correspond to the repeated expansion of the active area observed during one rotation of the wave. A similar modulation of an activation current on cobalt ribbon electrodes has been discussed in detail in ref. 16.

The phenomena on the ring can be discussed in the same way. The rotating active area can be considered as a section of the wave on the disk. The potential distribution depends sensitively on the exact position of the reference electrode. Considering the lack of reproducibility in positioning the Luggin capillary of the reference electrode, the potentials which have to be applied in order to observe a similar period of the rotation as in the case of the disk appear to be quite similar. Close inspection of Fig. 6(a) reveals changes in the curvature of the moving front depending on the position on the ring. Similar observations in the case of a catalytic surface reaction on a Pt ring have been explained by the anisotropy of the Pt surface.[25] While this explanation can be ruled out for the polycrystalline electrode surface, inhomogeneities on the metal surface or more likely a deviation from the circular symmetry, which can be seen on Fig. 6(a) and a possible off-centre position of the reference electrode may be responsible for modulating the shape and velocity of the wave front.

The reason for the appearance of a second wave at 950 mV *vs.* SCE is not clear at the present time. It may be due to surface inhomogeneities as has been pointed out for a catalytic surface reaction by Bär *et al.*[26] or to an intrinsic instability of the wave.

In the current–time series up to two frequencies can directly be observed in the experiments without [Fig. 3(b) and 6(b)] and with (Fig. 5 and 8) modulation of the wave. The lower frequency corresponds to the period of rotation and is probably due to a slightly asymmetric position of the reference electrode. The higher frequency observed in Fig. 3(b) could be due to the same modulation mechanism discussed above even though the expansion of the active area cannot be visually observed.

In electrochemical systems there is coupling through the electric field causing migration currents as was pointed out by Franck and Meunier.[27] Bell *et al.*[28] have shown that migration currents can play a major role in the coupling between two oscillating cobalt electrodes. Flätgen and Krischer[17,18] have shown how the non-local coupling can cause acceleration of electrochemical fronts owing to migration currents flowing parallel to the surface. This is a non-local, or long-range, coupling which exists in addition to the diffusive coup-

ling. Because the potential is not uniform throughout the electrolyte and therefore the coupling can decrease with position, the coupling is termed long-range rather than global. There is, of course, a smooth transition in the electrolyte.

The concept and the effect of non-local, or global, coupling has been demonstrated and analysed in a number of systems.

The effect of global coupling has been investigated experimentally and in a mathematical model for the NO + CO reaction on a Pt (100) surface by Veser *et al.*[29] and by Mertens *et al.*[30]

Rotating temperature waves propagating on a polycrystalline nickel ring during the oxidation of hydrogen at atmospheric pressure were reported by Lane and Luss.[31] Middya and co-workers[32,33] have shown how a global interaction caused by an integral constraint leads to spatiotemporal patterns. The effect of global interaction on reaction diffusion patterns generated from simulation using a simple cubic kinetic rate expression was investigated by the same authors.[34] Among other interesting phenomena, they have found one or several rotating pulses in a catalytic ring.

Concluding Remarks

Some similarities exist between spatiotemporal phenomena observed in a variety of systems and the experiments described in this paper, although, of course, the physical systems are quite different. In our work the parameter is the applied potential of the electrode and the non-local coupling leading to the observed spatiotemporal phenomena is due to the electric field. This causes migration currents parallel to the electrode surface and determines the electrode potential relative to the Flade potential and hence the stability of the passive oxide film.

The financial support for R. D. Otterstedt by the DAAD (grant No. D/94/05084) is gratefully acknowledged. The work was supported in part by grants from the National Science Foundation. We thank Yannis Kevrekidis and Bernie Matkowsky for very fruitful discussions and Jon Sayer for the digitization of the video images.

References

1 J. Woijtowicz, in *Modern Aspects of Electrochemistry*, ed. J. O'M Bockris and B. E. Conway, Plenum Press, New York, 1973, vol. 9, p. 47.
2 J. L. Hudson and T. T. Tsotsis, *Chem. Eng. Sci.*, 1994, **49**, 1493.
3 N. I. Jaeger, P. J. Plath and N. Q. Quyen, in *Temporal Order*, ed. L. Rensing and N. I. Jaeger, Springer Series in Synergetics, vol. 29, ed. H. Haken, Springer Verlag, Berlin 1984, p. 103.
4 M. Pagitsas, A. Karantonis and D. Sazou, *Electrochim. Acta*, 1992, **37**, 1047.
5 D. Sazou and M. Pagitsas, *J. Electroanal. Chem.*, 1992, **332**, 247.
6 D. Sazou and M. Pagitsas, *Electrochim. Acta*, 1995, **40**, 755.
7 Z. Noszticius, W. Horsthemke, W. D. McCormick, H. L. Swinney and W. Y. Tam, *Nature (London)*, 1987, **329**, 581.
8 M. M. Slin'ko and N. I. Jaeger, *Oscillating Heterogeneous Catalytic Systems, Stud. Surf. Sci. Catal.*, 1994, **86**.
9 O. Lev, M. Sheintuch, L. M. Pismen and Ch. Yarnitzky, *Nature (London)*, 1988, **336**, 458.
10 D. Haim, O. Lev, L. M. Pismen and M. Sheintuch, *J. Phys. Chem.*, 1992, **96**, 2676.
11 D. Haim, O. Lev, L. M. Pismen and M. Sheintuch, *Chem. Eng. Sci.*, 1992, **47**, 3907.
12 J. L. Hudson, J. Tabora, K. Krischer and I. G. Kevrekidis, *Phys. Lett. A*, 1994, **179**, 355.
13 J. C. Sayer and J. L. Hudson, *Ind. Eng. Chem. Res.*, 1995, **34**, 3246.
14 R.D. Otterstedt, N. I. Jaeger and P. J. Plath, *Int. J. Bifurcation Chaos*, 1994, **4**, 1265.
15 R. D. Otterstedt, P. J. Plath, N. I. Jaeger, J. C. Sayer and J. L. Hudson, *Chem. Eng. Sci.*, 1996, **51**, 1747.
16 R. D. Otterstedt, P. J. Plath, N. I. Jaeger and J. L. Hudson, *Phys. Rev. E.*, submitted.
17 G. Flätgen and K. Krischer, *Phys. Rev. E*, 1995, **51**, 3997.
18 G. Flätgen and K. Krischer, *J. Chem. Phys.*, 1995, **103**, 5428.
19 K. J. Vetter, *Elektrochemische Kinetik*, Springer Verlag, Berlin, 1961, p. 603.
20 A. Bayliss, B. J. Matkowsky and H. Rieke, *Physica D*, 1994, **74**, 1.
21 H. S. Brown and I. G. Kevrekidis, *Fields Institute Communications*, 1996, **5**, 45.
22 P. P. Russell and J. Newman, *J. Electrochem. Soc.*, 1987, **134**, 1051.
23 K. E. Heusler, *Corros. Sci.* 1965, **6**, 183.
24 U. F. Franck and R. FitzHugh, *Z. Elektrochem.*, 1961, **65**, 156.
25 M. D. Graham, M. Bär, I. G. Kevrekidis, K. Asakura, J. Lauterbach, H-H. Rotermund and G. Ertl, *Phys. Rev. E*, 1995, **52**, 76.
26 M. Bär, M. Eiswirth, H-H. Rotermund and G. Ertl, *Phys. Rev. Lett.*, 1992, **69**, 945.
27 U. F. Franck and L. Meunier, *Z. Naturforsch., Teil B*, 1953, **8**, 396.
28 J. C. Bell, N. I. Jaeger and J. L. Hudson, *J. Phys. Chem.*, 1992, **96**, 8671.
29 G. Veser, F. Mertens, A. S. Mikhailov and R. Imbihl, *Phys. Rev. Lett.*, 1993, **71**, 935.
30 F. Mertens, R. Imbihl and A. S. Mikhailov, *J. Chem. Phys.*, 1994, **101**, 9903.
31 S. L. Lane and D. Luss, *Phys. Rev. Lett.*, 1993, **70**, 830.
32 U. Middya and D. Luss, *J. Chem. Phys.*, 1994, **100**, 6386.
33 U. Middya, M. Sheintuch, M. D. Graham and D. Luss, *Physica D*, 1993, **63**, 393.
34 U. Middya, D. Luss and M. Sheintuch, *J. Chem. Phys.*, 1994, **100**, 3568.

Paper 6/01221C; *Received* 20*th February*, 1996